ELSEVIER

Finite Elements in Analysis and Design 38 (2002) 707–723

FINITE ELEMENTS IN ANALYSIS AND DESIGN

www.elsevier.com/locate/finel

Stress analysis of a helical gear set with localized bearing contact

Yi-Cheng Chen, Chung-Biau Tsay *

Department of Mechanical Engineering, National Chiao Tung University, 1001 Ta Hsueh Road, Hsinchu 30010, Taiwan, ROC

Abstract

This study investigates the contact stress and bending stress of a helical gear set with localized bearing contact, by means of finite element analysis (FEA). The proposed helical gear set comprises an involute pinion and a double crowned gear. Mathematical models of the complete tooth geometry of the pinion and the gear have been derived based on the theory of gearing. Accordingly, a mesh-generation program was also developed for finite element stress analysis. The gear stress distribution is investigated using the commercial FEA package, ABAQUS/Standard. Furthermore, several examples are presented to demonstrate the influences of the gear's design parameters and the contact positions on the stress distribution.

Keywords: Finite element stress analysis; Modified helical gear; Von-Mises stress; Bending stress; Hertzian contact stress

1. Introduction

Helical gears are widely used in power transmission between parallel shafts. Conventional parallel-axes helical gears with involute teeth are insensitive to center-distance assembly errors and possess line contacts under an ideal assembly condition. However, involute helical gears are very sensitive to axial misalignments, causing discontinuous transmission errors (TE) and edge contacts, resulting in noise and vibration [1]. Therefore, the teeth of helical gears are usually modified to attain a localized point contact and to avoid edge contacts. Recently, Litvin [2] proposed the concept of tooth surface modification to obtain a pre-designed parabolic TE as well as a localized bearing contact of the gear set. This concept of tooth modification has been applied to the generation of various kinds of gearing, such as spur gears, helical gears and worm gear drives [3–6].

* Corresponding author. Tel.: +886-3-5728-450; fax: +886-3-5728-450.
E-mail address: cbtsay@cc.nctu.edu.tw (C.-B. Tsay).

0168-874X/02/$ - see front matter
PII: S0168-874X(01)00100-7

The contact stress and fillet stress on gears, which are closely related to pitting failure, bending failure and the gear's service life, have attracted much attention [7,8]. Nevertheless, the calculation formulae for gears with special profile modifications are rarely available in handbooks [9,10]. Therefore, finite element analysis (FEA), which can involve complicated tooth geometry, is now a popular and powerful analysis tool to determine tooth deflections and stress distributions. Many researchers have applied FEA to tooth deflection and stress distribution for various gear drives. Several researchers have analyzed line-contact involute helical gears using three-dimensional (3-D) finite element (FE) stress analysis [7,8]. However, these researchers applied loads directly to the contact ellipses and contact lines obtained from tooth contact analysis (TCA).

Nevertheless, FE contact analysis for deformable bodies is complex and non-linear. Most early 3-D FE contact analyses were performed using gap elements [11]. Now, due to the progress of computer technology and computational techniques, some FEA packages can deal with contact analysis without using gap elements. Some researchers have begun to apply these FEA softwares to contact problems of gear surfaces [12,5].

This study adopts FEA to evaluate the stress distribution of a helical gear set with localized point contact. The gear set is composed of an involute pinion and a modified helical gear. The authors have presented a generation method for the modified helical gear, possessing double crowning effects in the profile and lengthwise directions [13]. This novel modified helical gear has been generated by adopting a generating tool with circular-arc normal sections instead of the conventional straight-edged sections, to attain the crowning effect on the gear profile direction. The generating tool moves along a curved-template guide on a hobbing machine to produce the crowning effect on the gear in the lengthwise direction. This study also derives the complete mathematical models for the pinion and the gear, including the working surfaces and the fillets, based on the theory of gearing and the generation mechanism. A computer program for the FE mesh generation of a 3-D tooth model is developed from the derived tooth geometry. An FEA package, ABAQUS, capable of contact analysis for two 3-D deformable bodies was employed to determine the stress distribution of a pair of contact gear teeth in point contact [14,15]. Finally, some numerical examples are presented to demonstrate the FE stress analyses under various design parameters and different contact positions.

2. Mathematical model of the modified helical gear set

The proposed helical gear set is composed of an involute pinion and a modified helical gear. The modified helical gear possesses both profile crowning and lengthwise crowning. Mathematical models of the pinion and the gear have been developed according to the theory of gearing [16,2] and the proposed generation mechanism [13,1]. For brevity, the equations are not derived in detail here.

2.1. Geometry of the involute helical pinion Σ_1

Gear generation by hob cutters can be simulated using an imaginary rack cutter [16,2]. According to Fig. 1(a), the normal section of the rack cutter surface Σ_P used to generate the involute pinion

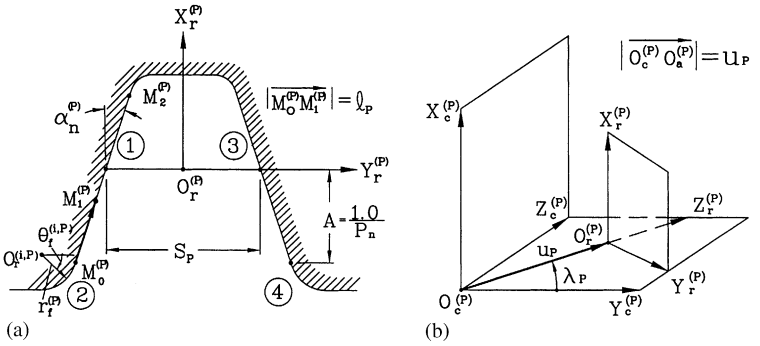

Fig. 1. Formation schema of rack cutter surface Σ_P.

surface, contains four major regions: two straight-edges (regions 1 and 3) and two circular curves (regions 2 and 4). Regions 1 and 3 generate the left-side and right-side involute screw surfaces of the helical pinion, while regions 2 and 4 generate the left-side and right-side fillets. Regions 1 and 2 are symmetric with regions 3 and 4, respectively, with respect to the $X_r^{(P)}$-axis. For simplicity, only the parameters of regions 1 and 2 are indicated in Fig. 1(a).

2.1.1. *Working surfaces of the involute helical pinion* Σ_1

Fig. 1(b) illustrates the relationship between coordinate systems $S_c^{(P)}$ and $S_r^{(P)}$, and the formation of the 3-D rack cutter Σ_P for the generation of an involute helical pinion. The working surfaces of the pinion are involute screw surfaces generated by straight cutting edges (regions 1 and 3) of rack cutter Σ_P. In Fig. 1, symbols ℓ_P and u_P stand for the parameters of the tool surface. Parameter A represents the pinion's dedendum, while S_P denotes the tooth space. Angles $\alpha_n^{(P)}$ and λ_P represent the normal pressure angle and the lead angle of the pinion, respectively. The position vector $\boldsymbol{R}_1^{(i)}$ of the working surfaces of Σ_1 can be represented as follows [1]:

$$x_1^{(i)} = (\ell_P \cos\alpha_n^{(P)} - A + r_1)\cos\phi_1 \pm (\ell_P \cos\alpha_n^{(P)} - A)\cot\alpha_n^{(P)} \sin\lambda_P \sin\phi_1,$$

$$y_1^{(i)} = (\ell_P \cos\alpha_n^{(P)} - A + r_1)\sin\phi_1 \mp (\ell_P \cos\alpha_n^{(P)} - A)\cot\alpha_n^{(P)} \sin\lambda_P \cos\phi_1,$$

and

$$z_1^{(i)} = \pm(A\tan\alpha_n^{(P)} - \ell_P \sin\alpha_n^{(P)})\cos\lambda_P \pm \left(\frac{A}{\cos\alpha_n^{(P)}\sin\alpha_n^{(P)}} - \frac{\ell_P}{\sin\alpha_n^{(P)}}\right)$$

$$\tan\lambda_P \sin\lambda_P \pm \frac{S_P}{2\cos\lambda_P} + r_1\phi_1\tan\lambda_P \quad i = 1 \quad \text{and} \quad 3. \tag{1}$$

The upper and lower signs refer to the left-side and right-side working surfaces, respectively. Parameter r_1 denotes the pinion's pitch radius and ϕ_1 is the pinion's rotational angle during its generation.

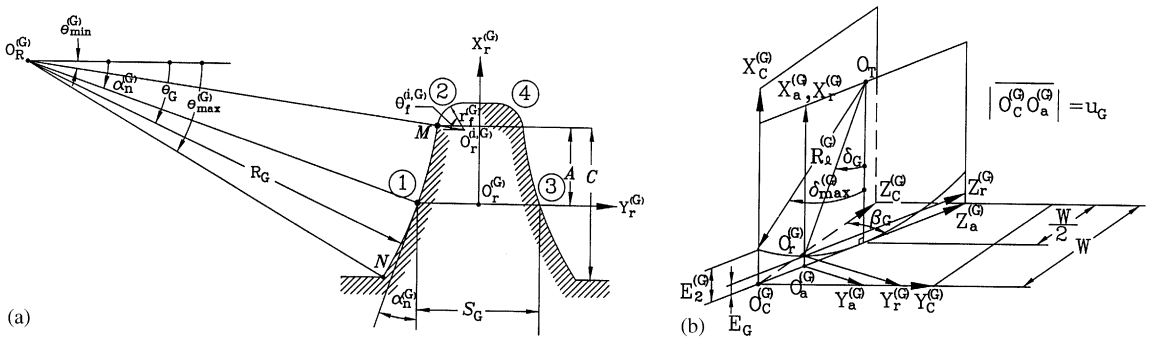

Fig. 2. Formation schema of rack cutter surface Σ_G.

2.1.2. Fillets of the involute helical pinion Σ_1

The fillets of the involute helical pinion are generated by regions 2 and 4 (circular curves) of rack cutter Σ_P. The equation of the fillets of the involute helical pinion are as follows:

$$\boldsymbol{R}_1^{(i)} = \begin{Bmatrix} (O_{rx}^{(i,P)} - r_f^{(P)} \sin\theta_f^{(i,P)} + r_1)\cos\phi_1 \pm (O_{rx}^{(i,P)} - r_f^{(P)} \sin\theta_f^{(i,P)})\cot\theta_f^{(i,P)} \sin\lambda_P \sin\phi_1 \\ (O_{rx}^{(i,P)} - r_f^{(P)} \sin\theta_f^{(i,P)} + r_1)\sin\phi_1 \mp (O_{rx}^{(i,P)} - r_f^{(P)} \sin\theta_f^{(i,P)})\cot\theta_f^{(i,P)} \sin\lambda_P \sin\phi_1 \\ -(O_{ry}^{(i,P)} \pm r_f^{(P)} \cos\theta_f^{(i,P)})\cos\lambda_P - \left(O_{ry}^{(i,P)} \pm O_{rx}^{(i,P)} \cot\theta_f^{(i,P)} - \dfrac{r_1\phi_1}{\sin\lambda_P}\right)\tan\lambda_P \sin\lambda_P \end{Bmatrix}$$

$$i = 2 \quad \text{and} \quad 4. \tag{2}$$

Similarly, the upper and lower signs refer to the left-side and right-side fillets, respectively. Here, $r_f^{(P)}$ denotes the radius of the fillet, and $\theta_f^{(i,P)}$ and u_P are parameters of the tool surface.

2.2. Geometry of the modified circular-arc helical gear Σ_G

Fig. 2(a) depicts the normal section of the rack cutter Σ_G applied to the generation of the modified helical gear, which comprises four major regions. Regions 1 and 3 generate the left-side and right-side working surfaces of the gear, while regions 2 and 4 generate the left-side and right-side fillets, respectively. Regions 1 and 2 are symmetric with regions 3 and 4, respectively, with respect to the $X_r^{(G)}$-axis. For simplicity, only the design parameters of regions 1 and 2 are shown in Fig. 2(a).

In practice, a curved-template guide can be employed on a conventional hobbing machine to produce a varied plunge of the hob cutter during gear generation. Fig. 2(b) illustrates the formation of the imaginary rack cutter surface Σ_G when a hob cutter moves with a varied plunge during the gear generation process. An auxiliary coordinate system $S_a^{(G)}(X_a^{(G)}, Y_a^{(G)}, Z_a^{(G)})$ which translates along the line $\overline{O_c^{(G)}O_a^{(G)}}$ (i.e. axis $Z_a^{(G)}$) is set up first. Line $\overline{O_c^{(G)}O_a^{(G)}}$ forms an angle β_G with axis $Z_c^{(G)}$ of the coordinate system $S_c^{(G)}(X_c^{(G)}, Y_c^{(G)}, Z_c^{(G)})$. The normal section of the circular-arc rack cutter is rigidly attached to coordinate system $S_r^{(G)}(X_r^{(G)}, Y_r^{(G)}, Z_r^{(G)})$ with its origin $O_r^{(G)}$ moving

along a curve of radius $R_\ell^{(G)}$. This curve has the same shape as the curved-template guide. The coordinate system $S_c^{(G)}(X_c^{(G)}, Y_c^{(G)}, Z_c^{(G)})$ is rigidly attached to the transverse section of the rack cutter. Therefore, coordinate system $S_r^{(G)}$ shifts by a variable amount, E_G, with respect to coordinate system $S_c^{(G)}$. Parameter δ_G indicates the position of point $O_r^{(G)}$ on the curved-template guide and E_G is the corresponding shift of the hob. Parameter $\delta_{max}^{(G)}$ denotes the extreme value of $\delta_{(G)}$ at which the parameter E_G reaches its maximum value $E_2^{(G)}$. Parameters W and β_G represent the face width and the helix angle of the gear, respectively.

The significant differences between the normal sections of Σ_P (Fig. 1(a)) and Σ_G (Fig. 2(a)) are the shapes of regions 1 and 3 which generate the working surfaces of tooth profiles. Regions 1 and 3 of the normal section of rack cutter Σ_G are circular arcs rather than straight lines, to produce tooth crowning in the profile direction of the generated gear. The deviation between the circular-arc and the straight line results in a built-in parabolic TE on the generated tooth surface. A curved-template guide is employed on a conventional hobbing machine to produce a varied plunge of the hob cutter during the gear generation process. Consequently, the varied shift-amount of the hob cutter causes a lengthwise crowning effect on the tooth flank to induce localized bearing contacts. Double crownings on the profile and lengthwise directions of the gear tooth surface are thus achieved on the modified helical gear.

2.2.1. Working surfaces of the modified circular-arc helical gear Σ_2

The left-side and right-side working surfaces of the modified circular-arc helical gear are generated by regions 1 and 3 of rack cutter surface Σ_G, respectively. The equations of the working surfaces can be expressed as follows [13]:

$$\boldsymbol{R}_2^{(i)} = \begin{Bmatrix} x_2^{(i)} \\ y_2^{(i)} \\ z_2^{(i)} \end{Bmatrix} = \begin{Bmatrix} (x_c^{(i,G)} - r_2)\cos\phi_2 + (y_c^{(i,G)} - r_2\phi_2)\sin\phi_2 \\ -(x_c^{(i,G)} - r_2)\sin\phi_2 + (y_c^{(i,G)} - r_2\phi_2)\cos\phi_2 \\ z_c^{(i,G)} \end{Bmatrix}, \quad i = 1 \quad \text{and} \quad 3, \tag{3}$$

and

$$\begin{aligned} f_2^{(i)}(\phi_2, \theta_G, \delta_G) = \Bigg\{ & \pm r_2\phi_2 + \left[R_G(\cos\alpha_n^{(G)} - \cos\theta_G) + \frac{S_G}{2} \right] \cos\beta_G \\ & \mp R_\ell^{(G)} (\sin\delta_{max}^{(G)} - \sin\delta_G)\sin\beta_G \Bigg\} \cos\delta_G \sin\theta_G \\ & + [R_G(\sin\alpha_n^{(G)} - \sin\theta_G) + R_\ell^{(G)}(1 - \cos\delta_G)] \\ & (\pm \sin\delta_G \sin\theta_G \sin\beta_G - \cos\delta_G \cos\theta_G \cos\beta_G) = 0, \quad i = 1 \quad \text{and} \quad 3. \end{aligned} \tag{4}$$

where $x_c^{(i,G)}$, $y_c^{(i,G)}$ and $z_c^{(i,G)}$ are expressed in the following:

$$\begin{aligned} x_c^{(i,G)} &= R_G(\sin\alpha_n^{(G)} - \sin\theta_G) + R_\ell^{(G)}(1 - \cos\delta_G), \\ y_c^{(i,G)} &= \mp \left[R_G(\cos\alpha_n^{(G)} - \cos\theta_G) + \frac{S_G}{2} \right] \cos\beta_G + R_\ell^{(G)}(\sin\delta_{max}^{(G)} - \sin\delta_G)\sin\beta_G, \end{aligned}$$

and

$$z_c^{(i,G)} = \pm \left[R_G(\cos \alpha_n^{(G)} - \cos \theta_G) + \frac{S_G}{2} \right] \sin \beta_G + R_\ell^{(G)}(\sin \delta_{max}^{(G)} - \sin \delta_G) \cos \beta_G. \tag{5}$$

The upper and lower signs represent the left-side and right-side working regions of Σ_2, respectively. Eq. (4) is the equation of meshing in the theory of gearing [16,2]. θ_G and δ_G are the surface parameters of rack cutter Σ_G. $\alpha_n^{(G)}$ is the normal pressure angle of the gear, while β_G represents the helix angle of the gear. S_G denotes the tooth thickness, R_G is the radius of the circular-arc cutting edges and $R_\ell^{(G)}$ denotes the radius of the curved-template guide used for lengthwise crowning. ϕ_2 is the gear's rotational angle during the generation process, and r_2 denotes the pitch radius of the gear.

2.2.2. Fillets of the modified circular-arc helical gear Σ_2

The left-side and right-side fillets of the modified circular-arc helical gear are generated by regions 2 and 4 of rack cutter Σ_G, respectively. Similarly, the position vector of the fillets can be represented by the following equations:

$$\boldsymbol{R}_2^{(i)} = \begin{Bmatrix} x_2^{(i)} \\ y_2^{(i)} \\ z_2^{(i)} \end{Bmatrix} = \begin{Bmatrix} (x_c^{(i,G)} - r_2)\cos\phi_2 + (y_c^{(i,G)} - r_2\phi_2)\sin\phi_2 \\ -(x_c^{(i,G)} - r_2)\sin\phi_2 + (y_c^{(i,G)} - r_2\phi_2)\cos\phi_2 \\ z_c^{(i,G)} \end{Bmatrix} \quad i = 2 \quad \text{and} \quad 4 \tag{6}$$

and

$$\begin{aligned} f_2^{(i)}(\phi_2, \theta_f^{(i,g)}, \delta_G) = \mp\{ & r_2\phi_2 - [(O_{ry}^{(i,G)} \mp r_f^{(G)} \cos\theta_f^{(i,G)})\cos\beta_G + R_\ell(\sin\delta_{max}^{(G)} \\ & - \sin\delta_G)\sin\beta_G]\}\cos\delta_G \sin\theta_f^{(i,G)} + [(O_{rx}^{(i,G)} + r_f^{(G)} \sin\theta_f^{(i,G)} + R_\ell(1 - \cos\delta_G)] \\ & \times (\mp \sin\delta_G \sin\theta_f^{(i,G)} \sin\beta_G + \cos\delta_G \cos\theta_f^{(i,G)} \cos\beta_G) = 0 \quad i = 2 \quad \text{and} \quad 4, \end{aligned} \tag{7}$$

where

$$\begin{aligned} x_c^{(i,G)} &= O_{rx}^{(i,G)} + r_f^{(G)} \sin\theta_f^{(i,G)} + R_\ell(1 - \cos\delta_G), \\ y_c^{(i,G)} &= (O_{ry}^{(i,G)} \mp r_f^{(G)} \cos\theta_f^{(i,G)})\cos\beta_G + R_\ell(\sin\delta_{max}^{(G)} - \sin\delta_G)\sin\beta_G, \end{aligned}$$

and

$$z_c^{(i,G)} = -(O_{ry}^{(i,G)} \mp r_f^{(G)} \cos\theta_f^{(i,G)})\sin\beta_G + R_\ell(\sin\delta_{max}^{(G)} - \sin\delta_G)\cos\beta_G. \tag{8}$$

The upper and lower signs indicate the left-side and right-side fillets of the modified circular-arc gear, respectively. $\theta_f^{(i,G)}$ and δ_G are the surface parameters of regions 2 and 4 of rack cutter Σ_G. Eq. (7) is the equation of meshing for the gear's fillets.

3. Finite element stress analysis

3.1. Finite element models and mesh generation program

This study adopts the general-purpose FEA software, ABAQUS/Standard operating on an HP workstation to evaluate the stress distribution of the proposed helical gear set. Since the commercial FEA package, ABAQUS/Standard, does not provide an interactive preprocessor, we have developed a mesh-generation program to establish FEA models for the pinion and the gear according to the tooth geometry given in the preceding sections. A linear brick element, C3D8, having eight nodes and six faces, is employed to discretize the geometric models of the pinion and the gear tooth surfaces [14,15]. The developed mesh-generation program allows the mesh density and the number of elements to be adjusted to meet specific requirements. The mesh-generation program can be applied to construct FEA models for other types of gear tooth surfaces by modifying the subroutine related to tooth geometry.

In general, a FEA model with a larger number of elements for FE stress analysis may lead to more accurate results. However, an FEA model of the whole gear drive is not preferred, especially considering the limit of computer memories and the need for saving computational time. This study establishes an FEA model of one pair of contact teeth for the helical gear set. Fig. 3 displays the mesh system of the pinion and the gear. Each FE tooth model is stacked by 34 unequally-spaced transverse sections in the tooth lengthwise direction. The regions where stress concentration may occur, such as the fillets and possible contact areas, are discretized by a finer mesh. Moreover, the contact points on the tooth surfaces under light load can be predicted accurately by TCA [16,2].

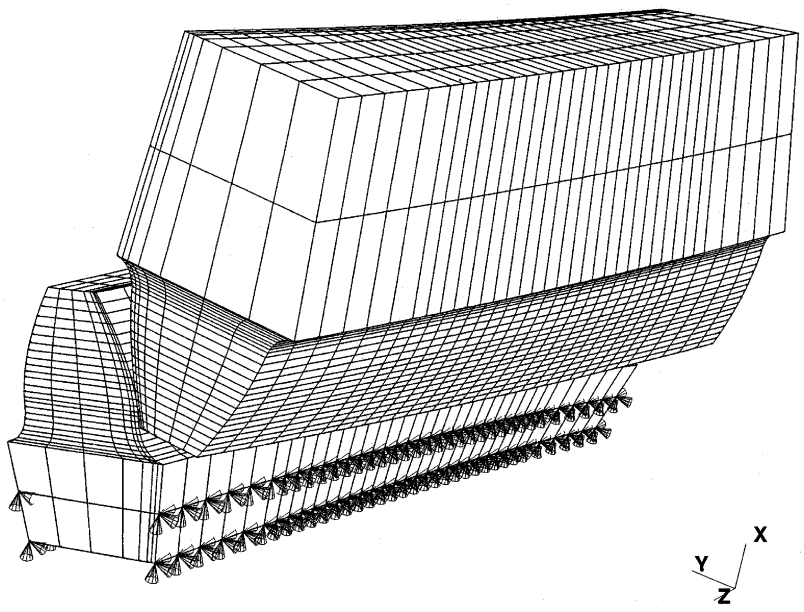

Fig. 3. Finite element model and boundary conditions of one pair of contact teeth.

Hence, the mesh density of the gear tooth middle sections is increased as shown in Fig. 3. In sum, 6188 elements and 7840 nodes are used for the pinion and the gear FE model, respectively.

3.2. Material properties and boundary conditions

Carbon steel has been chosen for the FEA model. Its basic mechanical properties are Young's Modulus $E = 207$ GPa and Poisson's Ratio $v = 0.292$. Fig. 3 displays the FE model of one pair of contact teeth and the applied boundary conditions. According to the FEA software, a linear brick C3D8 element is chosen, and each node has six degrees-of-freedom (DOF), including translations along the nodal x-, y- and z-directions and rotations about the nodal x-, y- and z-axes. In this study, all the six DOF of the nodes located on the two lateral sides of the pinion's base are fixed, as depicted in Fig. 3. On the other hand, rigid beam elements connect the nodes on the bottom of the gear's base with those on the gear's rotational axis. Furthermore, the nodes on the gear's rotational axis are constrained such that the gear can rotate only about its rotational axis. Consequently, the pinion is statically fixed and a torque is applied at the gear's rotational axis to make the gear and pinion tooth surfaces contact with each other.

3.3. Preliminary considerations and assumptions

In the contact stress analysis, the user must define the "contact pair" (the surfaces which may contact each other during the analysis) as the master and slave surfaces. Here, the master and slave surfaces are identified as the gear and the pinion tooth surfaces, respectively. During the analysis, the slave nodes cannot penetrate the master surface segments, but the nodes on the master surface may penetrate the slave surface segments. Additional contact elements are generated automatically during the analysis. Two other options, "small sliding" and "friction", should be specified to define the interaction between the contact surfaces. "Small sliding" is chosen in this study since it is computationally less expensive, especially in 3-D contact analyses. Coulomb friction is considered and the friction coefficient can be specified. This study assumes the gears to mesh under conditions of good lubrication, and the friction coefficient is given as zero.

Initially, the models are statically loaded by fixing the pinion and then applying a small torque to the gear member which makes the gear tooth contact the pinion tooth. The analyses proceed incrementally, and the contact between the two deformable bodies is handled automatically by imposing non-penetration constraints between the pinion and gear tooth surfaces.

In the FEA, a single pair of contact teeth is constructed to perform the stress analysis, and the following assumptions have been made: (1) the stress is in the elastic range of the material; (2) the material is isotropic; and (3) heat generation and thermal stress are ignored.

4. Illustrative examples

Table 1 summarized the design parameters of the proposed modified helical gear pair, composed of an involute pinion and a modified helical gear. In the FEA, a torque of 150 N m was applied to the gear's axis.

Table 1
Major design parameters of the proposed modified helical gear pair

Design values Parameters	Pinion	Gear
Number of teeth	18	36
Helix angle	15° (RH)	15° (LH)
Pressure angle, normal	20°	
Module, normal	4 mm	
Radius of curved-template guide $R_\ell^{(G)}$	Straight-edged	200 mm
Radius of rack cutter normal section R_G	Straight-edged	1000 mm
Face width	40 mm	

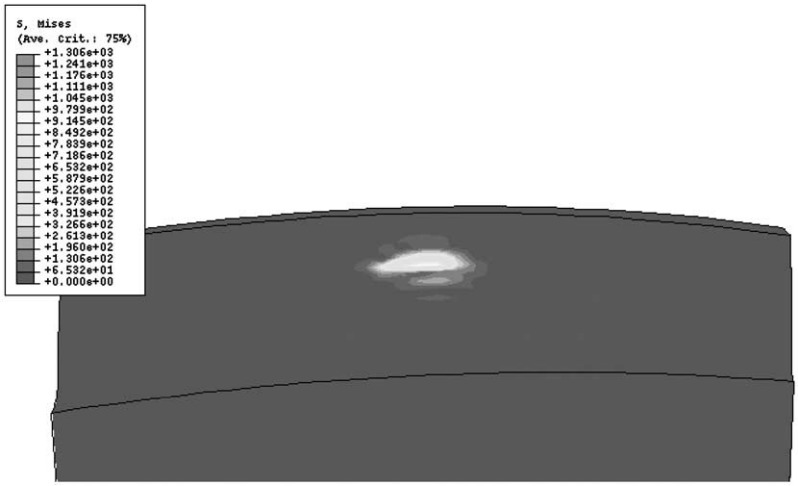

Fig. 4. Stress distribution on the gear.

4.1. Example 1: contact stress

According to the FE stress analysis simulation, Fig. 4 illustrates the distribution of von-Mises stress on the gear's tooth surface when the pinion's rotational angle is 0°. The maximum stress occurs at the contact position near the middle of the tooth flank. Based on the FEA results, the maximum principal stress is -1059.4 MPa, which is very close to the Hertzian contact stress, $\sigma_H = -1024.34$ MPa (calculated from Appendix A). Therefore, the proposed FEA method can be used to evaluate the contact stress.

4.2. Example 2: contact stress under different design parameters of gear crowning

Recall that for the double-crowned gear generation, parameter R_G indicates the radius of the rack cutter's normal section, while parameter $R_\ell^{(G)}$ denotes the radius of the curved-template guide

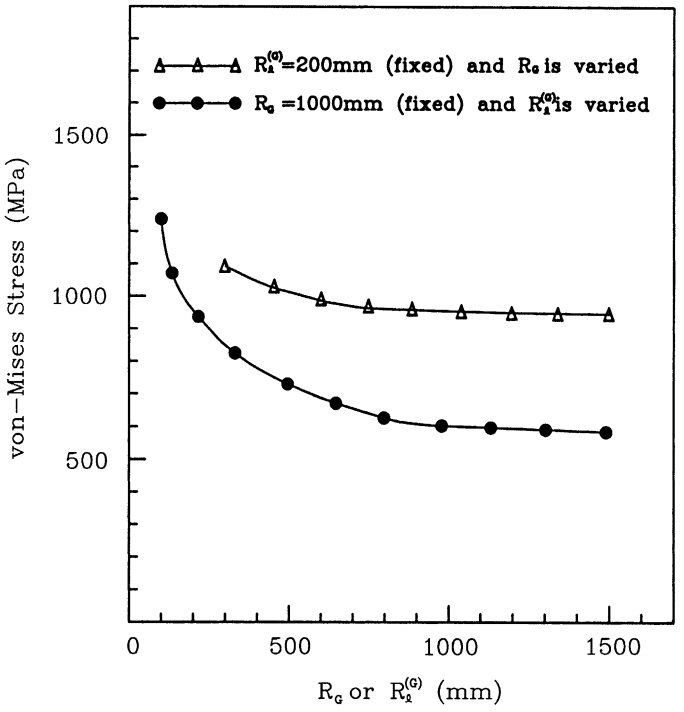

Fig. 5. The influence of parameters, R_G and $R_\ell^{(G)}$, on the maximum von-Mises stress of the gear.

along which the hob cutter moves during the generation process, as shown in Fig. 2. Therefore, R_G is related to the deviation of the generated tooth profile from the standard involute curve. The deviation results in a pre-designed parabolic TE of this helical gear set. On the other hand, $R_\ell^{(G)}$ affects the contact areas and the degree of lengthwise crowning is inversely proportional to $R_\ell^{(G)}$. Consequently, increasing the design parameter $R_\ell^{(G)}$ increases the contact area as well as a reduced contact stress.

According to the gear tooth mathematical model and the FEA results, Fig. 5 displays the maximum von-Mises stress on the gear under different design parameters of R_G and $R_\ell^{(G)}$. According to Fig. 5, when R_G is fixed at 1000 mm, the maximum von-Mises stress decreases as $R_\ell^{(G)}$ increases. Nevertheless, the influence of R_G on the contact stress is insignificant when compared with that of $R_\ell^{(G)}$.

4.3. Example 3: bending stress calculations

The fillet stresses are determined at four pinion's rotational angles, $\phi_1' = -5^\circ, 0^\circ, 5^\circ$ and 9°. As mentioned earlier, the FE models of the pinion and the gear have each been divided into 34 transverse sections, with the interface of the 17th and 18th transverse sections passing through the middle of the tooth flank. The theoretical contact point is at the 18th transverse section of the pinion and the gear tooth models, based on the TCA results. Accordingly, Figs. 6(a)–(d) demonstrate the stress

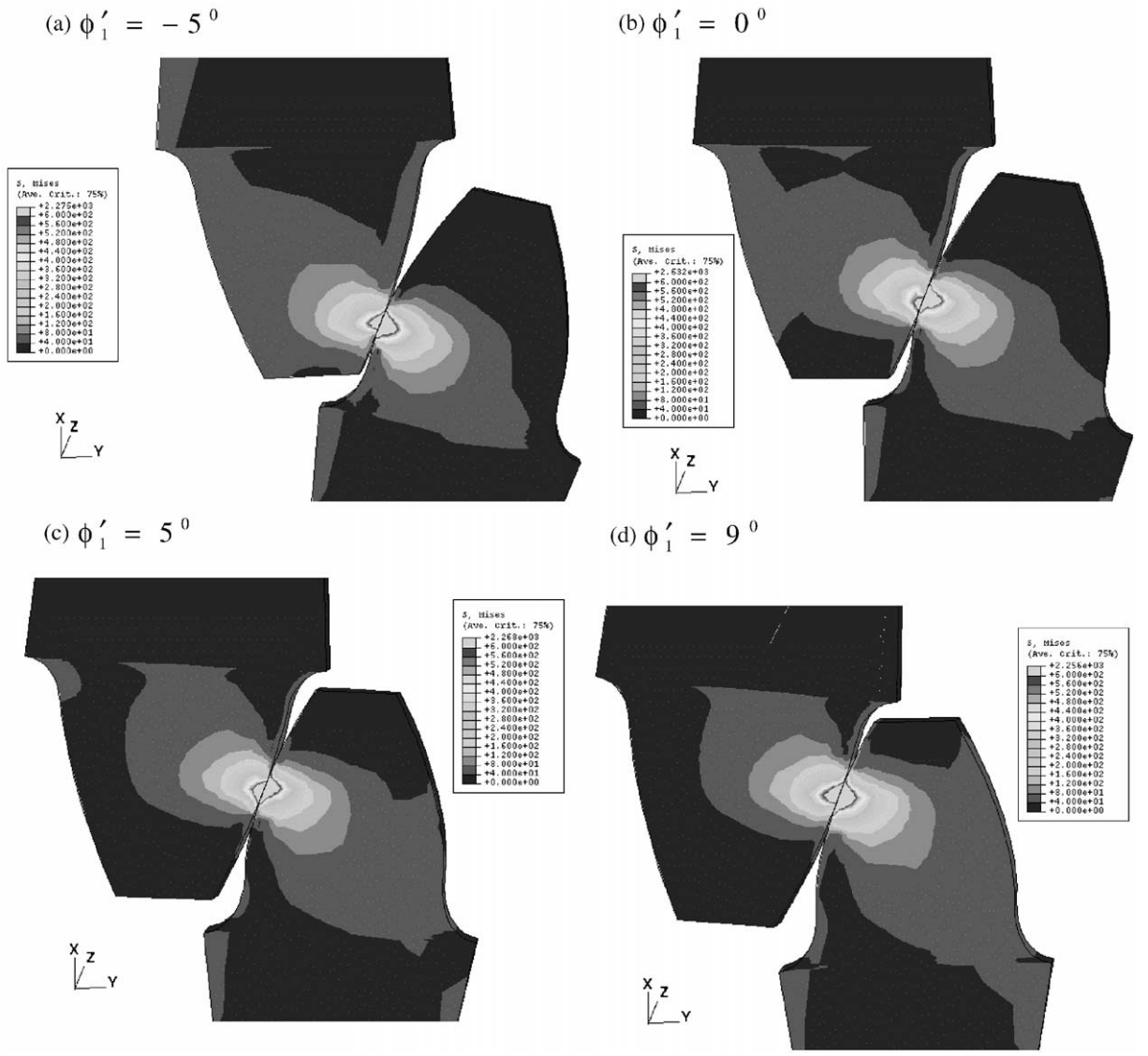

Fig. 6. Stress distribution on the 18th transverse section of the contact teeth under different contact positions.

distributions of the 18th transverse sections of the pinion and the gear, under these four contact positions. The variation of the bending stress is small because the bending stress in the fillet is much smaller than the contact stress.

Generally, the bending stresses in the fillets of the two contacting tooth sides are considered tensile stresses, and those in the fillets of the opposite, unloaded tooth side, are considered compressive stresses. Figs. 7(a) and (b) depict the tensile and compressive bending stresses along the pinion's fillet for the four contact positions. The bending stress is the average of von-Mises stresses at the eight integration points of the fifth element counted from the dedendum. As Fig. 7(a) shows, the

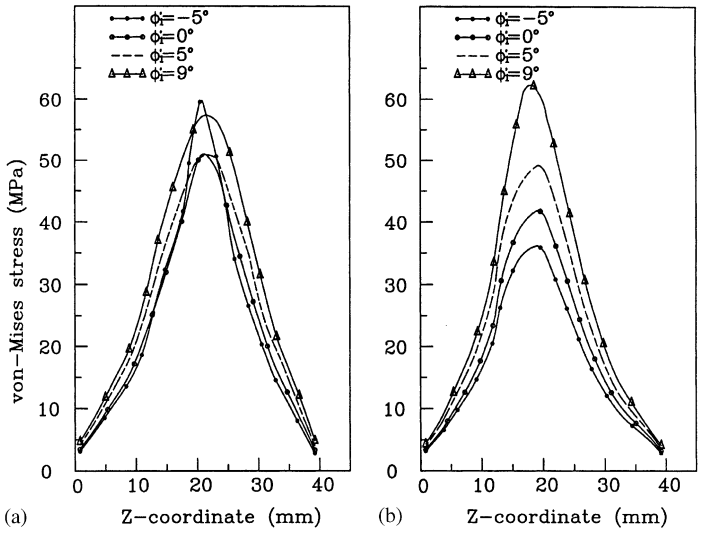

Fig. 7. Bending stress along the pinion's fillet.

maximum tensile bending stress occurs around the half-face width ($W/2 = 20$ mm), that is below the contact point, for each contact position. In the four contact positions, the maximum tensile bending stresses are 59.65, 50.64, 50.37 and 56.73 MPa. When $\phi_1' = -5^\circ$, as shown in Fig. 6(a), the contact point is close to the fillet and the tensile bending stress is high due to stress concentration. Furthermore, at $\phi_1' = 9^\circ$, the contact position is near the addendum of the pinion, exerting a large bending moment and a high bending stress on the tooth root. Therefore, the maximum tensile bending stresses under the two contact positions ($\phi_1' = -5^\circ$ and 9°) are higher than other positions ($\phi_1' = 0^\circ$ and 5°).

Figs. 6 (a)–(d) also illustrate that as the pinion rotates from -5° to 9°, the contact position moves upward from the dedendum to the addendum on the pinion, yielding a larger compressive bending stress on the opposite and unloaded sides. Therefore, the maximum compressive bending stresses increases as the pinion rotates from -5° to 9°, as is clear in Fig. 6(b). Furthermore, the respective peak values of the compressive fillet stresses under the four contact positions are 35.99, 41.8, 49.1 and 62.11 MPa.

4.4. Example 4: stress analysis of a conventional involute helical gear pair

In this example, the stress of a conventional involute helical gear pair is studied via FEA and American Gear Manufacturers Association (AGMA) stress formulae (please refer to Appendix B). Table 2 summarizes the major design parameters of the involute helical gear pair, and Fig. 8 displays the stress distribution on the pinion according to FEA results. Based on FEA results and Fig. 8, the von-Mises stress in the fillet of the pinion is 28.93 MPa for the involute helical gear pair. In addition, the maximum principal stress on the gear is 342 MPa based on the FEA results. On the other hand, the contact and bending stress numbers of the involute helical gear pair are calculated based on AGMA standard, AGMA 2101-C95 [17]. According to the AGMA stress formulae, the

Table 2
Major design parameters of the involute helical gear pair

Design values Parameters	Pinion	Gear
Number of teeth	17	35
Helix angle	20° (RH)	20° (LH)
Pressure angle, normal	20°	
Module, normal	4 mm	
Face width	40 mm	

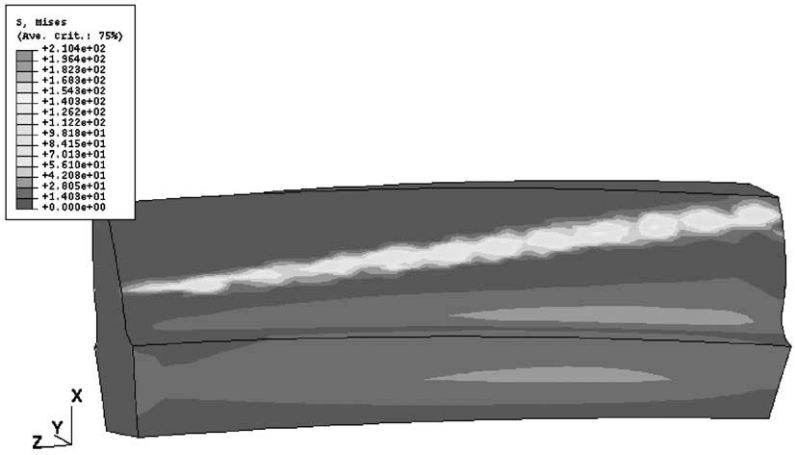

Fig. 8. Stress distribution on the pinion of the involute helical gear pair.

contact stress is 394.99 MPa and the bending stress on the pinion is 28.34 MPa. Therefore, the proposed FE stress analysis model for the modified helical gear pair yields reasonable results.

5. Conclusions

In this study, finite element stress analysis was performed to investigate the contact stress and the bending stress of a modified helical gear set comprising an involute pinion and a modified helical gear. The FEA tooth models including the working surfaces and the fillets of the pinion and the gear were developed. Commercial FEA software, ABAQUS/Standard, capable of contact analysis was applied to evaluate the stress distribution on the tooth surfaces. The analysis results leads to the following conclusions:

(1) The proposed helical gear set exhibits localized bearing contacts due to double crowning on the gear's tooth surfaces.

(2) The contact stress calculated by FEA is close to the Hertzian contact stress obtained from the Hertzian stress formulae and curvature analysis.

(3) Increasing $R_\ell^{(G)}$ results in an increase in the contact area and a reduction in contact stress, due to a smaller lengthwise crowning effect on the gear's tooth surfaces. Although a larger R_G causes a smaller profile crowning effect, the reduction of contact stress is less significant than the influence of $R_\ell^{(G)}$.

(4) The tensile and compressive bending stresses along the pinion's fillets under different contact positions were investigated. The maximum fillet stress occurs near the middle section of the tooth flank (below the contact points).

(5) Although this study investigated a modified helical gear set, the developed mesh generation program can also be applied to discretize FEA models for other types of gearing.

(6) The proposed FEA method can accurately calculate the contact and bending stresses. This model can be extended further to investigate the load share and transmission errors under load.

Acknowledgements

The authors would like to thank the National Science Council of the ROC for financially supporting this research under Contract No. NSC 89-2212-E-009-084.

Appendix A. Determination of Hertzian contact stress

The instantaneous contact point of the gear tooth surfaces is spread over an elliptical area with the center of symmetry located at the theoretical contact point, due to the elasticity. Tooth contact analysis can determine accurately the theoretical contact point under a light load [16,2]. Assume that a torque $\boldsymbol{T}$ is applied at the gear's rotational axis. The contact force $\boldsymbol{F}$ acting on the contact point can be determined by [18]

$$\boldsymbol{F} = \frac{\boldsymbol{T}}{(\boldsymbol{R}_2^* \times \boldsymbol{n}_2^*) \cdot \boldsymbol{a}^{(2)}}, \tag{A.1}$$

where $\boldsymbol{R}_2^*$ and $\boldsymbol{n}_2^*$ denote the position vector and the unit normal vector of the contact point represented in the gear's coordinate system, and $\boldsymbol{a}^{(2)}$ represents the unit vector of the gear's rotational axis.

According to Hertzian contact stress formulae, the semi-axis b of the contact ellipse and the maximum Hertzian stress σ_H can be estimated by

$$b = C_b \sqrt[3]{F\Delta} \tag{A.2}$$

$$\sigma_H = -C_\sigma \left(\frac{b}{\Delta}\right). \tag{A.3}$$

Coefficients C_b and C_σ can be determined using Figs. 14–6.7 and 14–6.8 in Refs. [19]. The auxiliary parameter Δ is defined as

$$\Delta = \frac{2(1-\nu^2)}{(A+B)E}, \tag{A.4}$$

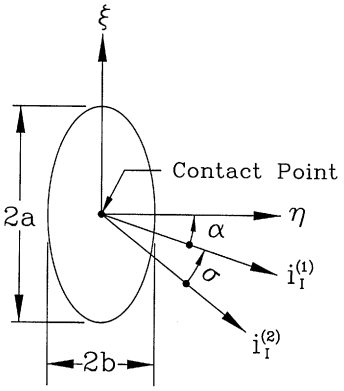

Fig. 9. Definition for orientation and dimension of a contact ellipse.

where v is the Poisson's ratio and E denotes the Young's modulus. A and B are determined by

$$A = \tfrac{1}{4}[\kappa_\Sigma^{(1)} - \kappa_\Sigma^{(2)} - (g_1^2 - 2g_1 g_2 \cos 2\sigma + g_2^2)^{1/2}], \tag{A.5}$$

$$B = \tfrac{1}{4}[\kappa_\Sigma^{(1)} - \kappa_\Sigma^{(2)} + (g_1^2 - 2g_1 g_2 \cos 2\sigma + g_2^2)^{1/2}], \tag{A.6}$$

where

$$\kappa_\Sigma^{(1)} = \kappa_I^{(1)} + \kappa_{II}^{(1)}, \tag{A.7}$$

$$\kappa_\Sigma^{(2)} = \kappa_I^{(2)} + \kappa_{II}^{(2)}, \tag{A.8}$$

$$g_1 = \kappa_I^{(1)} - \kappa_{II}^{(1)}, \tag{A.9}$$

and

$$g_2 = \kappa_I^{(2)} - \kappa_{II}^{(2)}. \tag{A.10}$$

Here, $\kappa_I^{(1)}$ and $\kappa_{II}^{(1)}$ represent the first and second principal curvatures of the pinion surface Σ_1, while $\kappa_I^{(2)}$ and $\kappa_{II}^{(2)}$ represent the first and second principal curvatures of the gear surface Σ_2, respectively.

As Fig. 9 shows, angle σ is measured counterclockwise from $\boldsymbol{i}_I^{(2)}$to $\boldsymbol{i}_I^{(1)}$ and can be evaluated by

$$\sigma = \tan^{-1}\left(\frac{\boldsymbol{i}_I^{(1)} \cdot \boldsymbol{i}_{II}^{(2)}}{\boldsymbol{i}_I^{(1)} \cdot \boldsymbol{i}_I^{(2)}}\right), \tag{A.11}$$

where $\boldsymbol{i}_I^{(1)}$ and $\boldsymbol{i}_{II}^{(1)}$ denote the unit vectors of the first and second principal directions for the pinion, while $\boldsymbol{i}_I^{(2)}$ and $\boldsymbol{i}_{II}^{(2)}$ represent the unit vectors of the first and second principal directions for the gear, respectively.

Furthermore, the principal directions and the principal curvatures of the pinion and the gear tooth surfaces, and the orientation of the contact ellipses can be determined according to the differential geometry and Litvin's approach [16,2].

Appendix B. AGMA stress formulae

The contact stress and bending stress of gears are called "contact stress number" and "bending stress number" in AGMA standards. According to AGMA 2101-C95, the contact stress number σ_H and the bending stress number σ_F for involute helical gears can be determined as follows [17]:

$$\sigma_H = Z_E \sqrt{F_t K_o K_v K_s \frac{K_H}{2r_1 W} \frac{Z_R}{Z_I}}, \tag{B.1}$$

and

$$\sigma_F = F_t K_o K_v K_s \frac{1}{W m_t} \frac{K_H K_B}{Y_J}, \tag{B.2}$$

where F_t is the transmitted tangential load, K_o is the overload factor, K_v is the dynamic factor, K_s is the size factor, K_H is the load distribution factor, K_B is the rim thickness factor, Z_E is the elastic coefficient, Z_R is the surface condition factor, r_1 denotes the pitch radius of the pinion, W is the face width and m_t is the transverse module. Parameters Z_I and Y_J denote the geometry factors for pitting resistance and for bending strength, respectively. The detailed derivations and Tables of geometry factors Z_I and Y_J are included in AGMA 908-B89 [20]. According to the design parameters of the involute helical gear pair listed in Table 2, the geometry factor Z_I is 0.177, and the values of geometry factor Y_J are 0.46 and 0.51 for the pinion and the gear, respectively.

References

[1] C.B. Tsay, Helical gears with involute shaped teeth: geometry, computer simulation, tooth contact analysis, and stress analysis, ASME J. Mech. Transmissions Automation Des. 110 (1988) 482–491.
[2] F.L. Litvin, Gear Geometry and Applied Theory, Prentice-Hall, U.S.A., New Jersey, 1994.
[3] F.L. Litvin, D.H. Kim, Computerized design, generation and simulation of modified involute spur gears with localized bearing contact and reduced level of transmission errors, ASME J. Mech. Des. 119 (1997) 96–100.
[4] F.L. Litvin, N.X. Chen, J. Lu, R.F. Handschuh, Computerized design and generation of low-noise helical gears with modified surface topology, ASME J. Mech. Des. 117 (1995) 254–261.
[5] F.L. Litvin, Q. Lian, A.L. Kapelevich, Asymmetric modified spur gear drives: reduction of noise, localization of contact, simulation of meshing and stress analysis, Comput. Method Appl. Mech. Eng. 188 (2000) 363–390.
[6] Y. Zhang, Z. Fang, Analysis of transmission errors under load of helical gears with modified tooth gears, ASME J. Mech. Des. 119 (1997) 120–126.
[7] M.A.S. Arikan, M. Tamar, Tooth contact and 3-D stress analysis of involute helical gears, ASME, International Power Transmission and Gearing Conference, De-Vol. 43, No. 2, 1992, pp. 461–468.
[8] C.R.M. Roa, G. Muthuveerappan, Finite element modelling and stress analysis of helical gear teeth, Comput. Struct. 49(6) (1993) 1095–1106.
[9] E. Buckingham, Analytical Mechanics of Gears, Dover, U.S.A., New York, 1949.
[10] D.W. Dudley, Dudley's Gear Handbook, 2nd Edition, McGraw-Hill, U.S.A., New York, 1992.
[11] I.H. Filiz, O. Eyercioglu, Evaluation of gear tooth stresses by finite element method, ASME J. Mech. Des. 117 (1995) 232–239.
[12] R.F. Handschuh, G.D. Bibel, Experimental and analytical study of aerospace spiral bevel gear tooth fillet stresses, ASME J. Mech. Des. 121 (1999) 565–572.
[13] Y.C. Chen, C.B. Tsay, Mathematical model and undercutting analysis of modified circular-arc helical gears, J. Chinese Soc. Mech. Eng. 22(1) (2000) 41–51.
[14] ABAQUS/Standard 5.8, User's Manual, Hibbitt, Karlsson & Sorensen U.S.A, 1998.

[15] R.D. Cook, D.S. Malkus, M.E. Plesha, Concepts and Applications of Finite Element Analysis, 3rd Edition, Wiley, U.S.A., New York, 1989.
[16] F.L. Litvin, Theory of Gearing, NASA Publication RP-1212 U.S.A., Washington, DC, 1989.
[17] American Gear Manufacturers Association, AGMA 2101-C95, Fundamental rating factors and calculation methods for involute spur and helical gears, U.S.A, 1994.
[18] F.L. Litvin, J.S. Chen, J. Lu, R.F. Handschuh, Application of finite element analysis for determination of load share, real contact ratio, precision of motion, and stress analysis, ASME J. Mech. Des. 118 (1996) 561–567.
[19] A.P. Boresi, O.M. Sidebottom, Advanced Mechanics of Materials, 4th Edition, Wiley, U.S.A., New York, 1985.
[20] American Gear Manufacturers Association, AGMA 908-B89, Geometry factors for determining the pitting resistance and bending strength of spur, helical and herringbone gear teeth, U.S.A, 1989.